Incorporation and migration of hydrogen in yttria-stabilized cubic zirconia: Insights from semilocal and hybrid-functional calculations

A. G. Marinopoulos

CEMDRX and Physics Department, University of Coimbra, Rua Larga, 3004-516 Coimbra, Portugal

(Received 22 July 2012; revised manuscript received 17 September 2012; published 24 October 2012)

Hydrogen is a common impurity in oxides and is known to exhibit dual behavior: It can act either as a dopant or alternatively as a compensating impurity, depending on whether its transition (pinning) level, $E(+/-)$, intersects the conduction band or lies deep in the energy gap. In the present work the incorporation of isolated hydrogen in 10.3 mol% yttria-stabilized zirconia was studied by *ab initio* calculations employing a semilocal exchange-correlation density functional and a hybrid-functional approach. Equilibrium sites and formation energies were determined for the different charged states of hydrogen and the role of intrinsic oxygen vacancies needed to stabilize the cubic phase of the oxide was particularly examined. Hydrogen was found to be an amphoteric impurity with the equilibrium charge-transition levels, $E(q,q')$, lying deep inside the gap. Whereas, in its positively charged state, H^+, hydrogen was found exclusively to form a dative-type bond with the lattice oxygens, the negatively charged and neutral states also adopt interstitial configurations provided by the empty cubes and the intrinsic structural vacancies of the anion sublattice. Two distinct paramagnetic configurations of hydrogen, H^0, are predicted and both of them induce deep localized levels in the band gap. The first configuration is higher-energy compact atomlike with the hydrogen at the interstitial sites, whereas the second one is a bond-type deep donor configuration with the unpaired $4d$ electron localized predominantly at an undercoordinated Zr cation in the vicinity of the impurity. Minimum-energy paths and corresponding classical barriers of migration were also determined for H^0 with the aid of the nudged elastic-band method providing insight on the feasibility of site interplay of H^0 and interconversion among its interstitial and donor configurations. Oxygen vacancies and lattice relaxation were found to have a major effect on the energy profiles of the paths, the position of the transition states, and the magnitude of the migration barriers.

DOI: 10.1103/PhysRevB.86.155144 PACS number(s): 61.72.−y, 71.15.Nc, 71.20.−b, 71.55.−i

I. INTRODUCTION

Hydrogen is a ubiquitous impurity in technological materials and devices. It is often incorporated intentionally with the goal to achieve beneficial effects, in particular by passivating defect-related trap centers. Nonetheless, it can also be involved in serious reliability issues such as the bias-temperature instability in metal-oxide-semiconductor devices and radiation-induced degradation processes.[1–4] *Ab initio* calculations based on density-functional theory[5] (DFT) have played a pivotal role in our present understanding of hydrogen configurations in semiconductors and insulators as well as of its reactions and complexing with intrinsic defects and dopants.[4,6–16] One of the goals in these DFT studies has also been to predict the behavior of isolated hydrogen in terms of its electrical activity, namely whether it can act as dopant or alternatively as an amphoteric impurity counteracting the prevailing conductivity in the host material.[9–14,17]

For the case of cubic yttria-stabilized zirconia (YSZ), a fast ionic conductor commonly used as solid electrolyte in electrochemistry, a number of recent experimental findings require a rigorous understanding of how hydrogen incorporates in the YSZ lattice either as a proton or in its neutral paramagnetic state: High protonic conductivity was reported in bulk polycrystalline YSZ samples[18] and YSZ nanograin thin films[19] and a spectroscopic study of its muonium counterpart in bulk 9.5 mol% cubic YSZ uncovered signatures of both shallow-donor and compact atomlike configurations.[20]

The latter work represents a detailed survey[20] of isolated hydrogen states in wide-gap oxides, exploiting muon-spin rotation (μSR) spectroscopy using muonium, a light pseudoisotope of hydrogen with an electron bound to a positive muon. In a number of these oxides, including cubic YSZ, shallow-donor muonium states were observed to coexist at low temperatures with atomic paramagnetic states of high hyperfine constants. At and above room temperature the subsequent loss of the paramagnetic fraction, Mu^0, suggested a conversion towards the diamagnetic muonium states (Mu^+ or Mu^-). While μSR spectroscopy detects paramagnetic and diamagnetic states with equal sensitivity,[21–26] it more easily identifies the neutral paramagnetic states via their distinctive hyperfine couplings.[20] The ionic states Mu^+ and Mu^-, on the other hand, could not be unambiguously distinguished in the μSR data of Ref. 20, so that the chemical identity of the high-temperature diamagnetic component remains uncertain. Derived activation energies of the conversion process of the atomic muonium were only reported[20] for the monoclinic phase of zirconia (0.23 and 0.82 eV) adding to the uncertainty for the case of the cubic YSZ phase. As discussed in Ref. 20 hole ionization or second-electron capture would suggest a conversion of Mu^0 to Mu^-; assigning therefore the reported activation energies to acceptor levels, $E(0/-)$, would place the latter low in the band gap. An alternative possibility also proposed is a possible site change that combined with electron ionization would lead to thermal conversion of Mu^0 to the positive ion, Mu^+.

These observations and analyses of the μSR measurements raise a number of important questions regarding the presence of isolated hydrogen in cubic YSZ. It is, therefore, important to determine the locations where hydrogen resides in the

lattice depending upon its charge state and furthermore the range of stability of these charge states for varying Fermi-level positions in the gap through the corresponding charge-transition levels. Insight on the migration behavior of the neutral paramagnetic state of hydrogen, H^0, is also needed in order to understand possible site interplay for H^0 and interconversion among its distinct components.

In the present work the incorporation and energetics of interstitial hydrogen in 10.3 mol% cubic YSZ was studied by means of *ab initio* calculations. These included density-functional[5] calculations using the semilocal PBE (Perdew, Burke, and Ernzerhof) functional[27] obtained within the generalized-gradient approximation (GGA) for exchange and correlation as well as a hybrid-functional approach due to Heyd, Scuseria, and Ernzerhof.[28–30] Hybrid functionals partially reduce the self-interaction error[31] and correct the delocalization bias of standard DFT functionals by admixing a certain part of nonlocal Hartree-Fock exchange to the local or semilocal DFT exchange.[29,30] They were shown to provide improved results for solids in terms of both structural properties and energy band gaps.[29,30] In recent *ab initio* studies of hydrogen and other defects in semiconductors and oxides hybrid functionals have given more accurate results of defect-formation energies and charge-transition levels with respect to local or semilocal DFT functionals.[26,32–42]

The theoretical and computational framework adopted in the present study is described in Sec. II. Specific details are also presented on the atomistic structural models for YSZ that were used for the defect calculations. Section III contains the first part of results where the multiple minimum-energy configurations of hydrogen in its different charge states are presented, together with their formation energies as a function of the Fermi-level position in the gap. Special attention was also given to the position and character of the defect-induced levels for the neutral paramagnetic state of hydrogen, H^0, for which the existing μSR data[20] inferred two distinct components, one atomlike with high hyperfine constant and a second one acting as a shallow donor. Section IV contains the results on the global stability and migration energetics of the H^0 state in the lattice. These calculations were performed exclusively using the DFT PBE functional and were based on the nudged elastic-band (NEB) method.[43] The aim has been to identify the possible site changes of H^0 among the nonequivalent paramagnetic H^0 configurations in the lattice and their feasibility through the calculated minimum-energy paths (MEPs) and related classical barriers of migration. Specific migration mechanisms and paths that lead to the equilibrium donor location, the geometrical site that hydrogen occupies in both its neutral and its positively charged states, were found and discussed, examining the roles of the oxygen vacancies and of lattice relaxation.

II. THEORETICAL BACKGROUND AND PRELIMINARIES

The majority of the calculations in the present study were based on spin-polarized DFT[5] and the projector-augmented wave (PAW) method[44,45] and were performed within the GGA for exchange and correlation. More specifically, the semilocal PBE (Perdew, Bethe, Ernzerhof) functional[27] was used. For this purpose, the corresponding implementations of the VASP code[46–48] were employed. The crystalline wave functions were expanded in a plane-wave basis limited by a cutoff energy of 470 eV. For both zirconium and yttrium atoms the semicore $4s$ and $4p$ electrons were included in the valence states. For the defect calculations, a Monkhorst-Pack[49] $2 \times 2 \times 2$ mesh was chosen for the Brillouin-zone integrations.

In the present work the hybrid HSE06 functional due to Heyd, Scuseria, and Ernzerhof[28–30] was employed, again as implemented in the VASP code where the Hartree-Fock exchange is calculated under periodic boundary conditions. A mixing fraction of 0.25 was chosen and found to provide energy band gaps in satisfactory agreement with experimental data. Through the introduction of a screening length, nonlocal Hartree-Fock exchange is added in the short-range part of the potential, whereas the long-range exchange potential and correlation are both described by the PBE functional.

The present calculations of interstitial hydrogen in YSZ were performed on a fluorite-based 96-atom zirconia supercell with 10.3 mol% yttria concentration. Starting from the simple cubic cell of zirconia the supercell was generated by doubling the cell dimensions along the cubic lattice vectors. Before doping, the volume of the fluorite primitive cell was independently optimized by both the PBE and the hybrid-functional approaches. The obtained lattice parameters, a_o, for these undoped fluorite lattices were found to be equal to 5.149 and 5.105 Å, respectively. The desired yttria concentration was achieved by introducing six yttrium atoms substitutionally in the Zr sublattice together with the necessary (three) charge-compensating oxygen vacancies. No additional oxygen vacancies or other intrinsic defects were introduced.

The final lattice parameters, a_{latt}, for the YSZ supercells were accordingly adjusted to account for the yttria doping.[50] The experimentally derived expression[51] for the lattice parameters was used, $a_{\text{latt}} = a_o + 0.003x$ (in Å), which gives the observed increase of the lattice parameter of YSZ with increasing yttria content x (in mol%) and a_o being the extrapolated parameter at zero yttria concentration.

With the goal to obtain stable low-energy YSZ supercells a total of 17 trial configurations were initially constructed with a variety of oxygen-vacancy arrangements. Defect association was also considered: Substitutional yttrium atoms were in most cases placed at next (second)-nearest-neighbor positions (NNN) with respect to the oxygen vacancies. This defect association was confirmed by the present and past DFT calculations[50,52–56] to lead to lower-energy YSZ supercells. Furthermore, recent experimental studies of extended x-ray absorption fine-structure spectroscopy[57–59] and nuclear magnetic resonance[60] that probed the local coordination of yttrium ions in YSZ also suggested a NNN yttrium-vacancy association.

The structural optimization carried out by the PBE functional for all trial supercell configurations showed that the final (relaxed) supercells comprised the following vacancy-vacancy configurations in order of increasing vacancy-vacancy separation: The closest vacancy-vacancy pairs were second-nearest (seven supercells), third-nearest (four supercells), and fifth-nearest (six supercells) neighbors. All trial cells with vacancies at nearest-neighbor sites of the anion sublattice were found to be unstable and transformed to other structures. The lowest-energy configuration was obtained when oxygen vacancies were at least fifth-nearest neighbors with the yttrium

ions positioned at NNN sites with respect to the vacancies. This YSZ cell was employed for the hydrogen calculations in the present study. Nonetheless, other configurations with vacancies at closer distances such as ⟨111⟩ divacancy pairs were also found to be stable, albeit of higher energies. Selected calculations with hydrogen introduced in one of these higher-energy cells were also carried out; the results of these calculations (for eight distinct hydrogen positions) confirmed that the observed trends concerning the energetics of hydrogen incorporation, the type of equilibrium sites of hydrogen, and nature of defect levels in the gap do not depend upon the choice of the supercell and the specific vacancy arrangement.

The formation energies $E_{\text{form}}(H^q)$ of the different configurations of hydrogen for every charge state ($q = -1$, 0, and $+1$) were determined for either approach discussed above. $E_{\text{form}}(H^q)$ depends upon the Fermi-level position, E_F, in the gap and the chemical potential, μ_H, of hydrogen. The energy of the valence-band maximum (VBM), E_{VBM} of the bulk supercell was taken as the reference energy for the charged states of the impurity. The expression is

$$E_{\text{form}}(H^q) = E_{\text{tot}}(H^q) - E_{\text{tot}}(\text{bulk}) - \mu_H + q(E_F + E_{\text{VBM}}), \quad (1)$$

where $E_{\text{tot}}(H^q)$ and $E_{\text{tot}}(\text{bulk})$ are the total energies of the supercell containing the hydrogen and the bulk-crystal supercell, respectively. In the present work, μ_H was taken as half the total energy of the hydrogen molecule. Accordingly, the charge-transition levels, $E(q/q')$, are formally defined as the E_F positions in the gap where the formation energies of charge states q and q' are equal. Therefore, these levels mark the stability limits of the different charge states of hydrogen in the gap. For the charged configurations, a homogeneous charge background was always added to ensure charge-neutral cells. Electrostatic corrections originating from the interactions of the defects with their periodically created images[61] were also calculated and found to be of the order of 0.1 eV.

The MEPs and associated migration energies for the neutral state of hydrogen were determined by the NEB method[43] using solely the PBE functional. The zero-point energy of hydrogen at its various configurations was also determined in the harmonic approximation through the diagonalization of the local dynamical matrix associated with the impurity.

III. HYDROGEN INCORPORATION IN THE YSZ LATTICE

A. Stable sites and formation energies

The stable sites of hydrogen in the different crystalline phases of zirconia have already been the subject of *ab initio* studies: in the ground-state monoclinic[42,62,63] and the higher-energy undoped tetragonal[62] and cubic[11,12,17,62] phases. More specifically, hydrogen in the undoped cubic zirconia lattice was studied by means of both semilocal DFT calculations[11,12,62] and calculations[17] within the weighted-density approximation for exchange and correlation that includes a portion of nonlocal exact exchange. In these studies hydrogen was found to form a dative-type bond with the oxygen ions by breaking a host Zr-O bond in the process. The defect level of the neutral impurity state was found to occupy the bottom of the conduction band; therefore, effectively atomic hydrogen donates its electron to the oxide conduction band and becomes ionized.

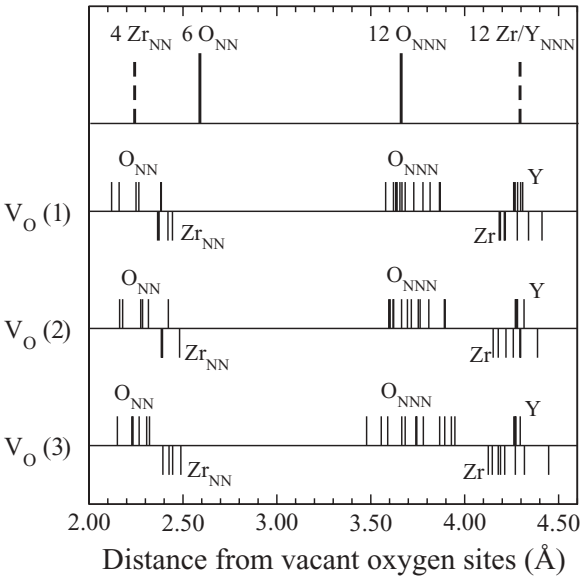

FIG. 1. Distances from the three vacant oxygen sites (V_O) for the ions of the neighboring shells (relaxed YSZ supercell). The top panel shows the number of neighbors and their distances for the case of the ideal (unrelaxed) fluorite cell.

In contrast to the ideal cubic fluorite structure, the YSZ structure possesses certain complexities. Despite the fact that the overall cubic structure is maintained, doping induces structural disordering to the cubic lattice with the largest local distortions from cubic symmetry taking place near the oxygen vacancies. The detailed ionic displacements after relaxation for both sublattices are shown in Fig. 1 as a function of the distance of the ions from the three introduced oxygen vacancies (denoted as V_O in the figure and in the remainder of the paper). It can be seen that the largest displacements take place near the vacancies. These severe localized displacements appear to suppress the tetragonal distortion of the oxygen sublattice that could potentially destabilize the cubic phase.[64]

The present calculations, similarly to earlier DFT results,[50,56] showed that the oxygen ions O_{NN} that are closest to the oxygen vacancies are displaced the most. These anions (six per vacancy) display a strong attraction towards the nearest-neighbor oxygen vacancies with the dominant component of their displacements along the cubic ⟨100⟩ directions [see Fig. 2(a)]. For the specific YSZ cell used in the defect calculations the magnitude of the displacements of these anions were in the range of 0.22–0.56 Å (see Fig. 3). Therefore, these oxygen ions do not reside in a perfect tetrahedral environment as in the ideal cubic lattice: In most cases their fourth Zr neighbor is found at distances beyond 3 Å and this effectively reduces their cation coordination number to three [see Fig. 2(a)]. On the other hand, the displacements of the more distant (to the vacancies) anions (denoted as $O_{>NN}$ in Fig. 3) were consistently smaller (0.12–0.30 Å) with a clear tendency for most next-nearest-neighbor anions (O_{NNN}) to displace further away from the vacant sites (see Fig. 1).

Smaller displacements are predicted for the heavier Zr cations; those cations that are nearest neighbors to the

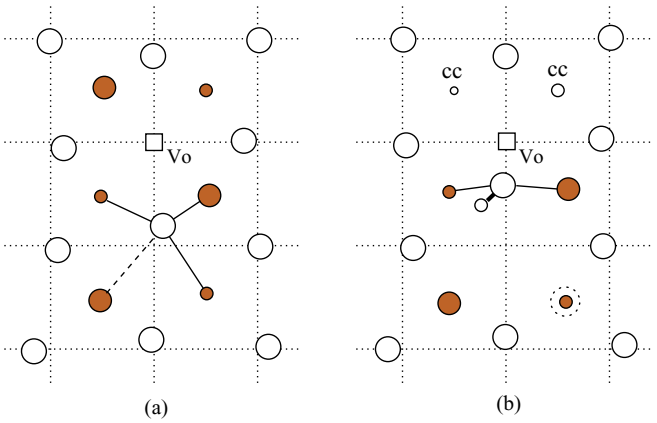

FIG. 2. (Color online) Structure of the 10.3 mol% YSZ lattice near an oxygen vacancy V_O (square symbol). The figure depicts a planar cut of an anion (001) plane. The dotted lines specify the unperturbed anion network of the undoped cubic-fluorite zirconia. (a) Bulk crystal. Solid lines connect the nearest Zr neighbors to the specified oxygen ion. The dashed line is used to indicate the Zr ion displaced further away from the central oxygen ion. (b) Representative minimum-energy hydrogen sites in the lattice. Sites denoted by cc are the cube-centered interstitial sites. A bond-type configuration is depicted explicitly by showing the covalent OH^- bond (thick solid line). Open (solid) circles denote oxygen (zirconium) ions. The smaller unfilled circles represent hydrogen sites. Different sizes for Zr and H denote different locations along the [001] viewing direction. For the meaning of the circled Zr cation (by the dotted circle), see text.

vacancies (Zr_{NN}) were all observed to be repelled from the vacancies (see Fig. 1) and were displaced the most with displacements in the range of 0.13–0.25 Å. The introduced yttrium ions, on the other hand, exhibited considerably smaller displacements during relaxation and continued to occupy NNN positions with respect to the vacancies, at least 4 Å away (see Fig. 1). The observed displacement patterns for the two

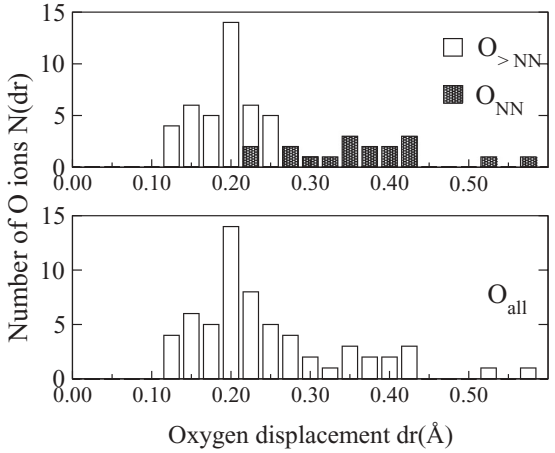

FIG. 3. The histograms depict the magnitude of the displacements dr for all oxygen ions in the YSZ supercell. The ideal fluorite (unrelaxed) structure is taken as the reference configuration. The top panel shows separately the displacements for those anions which are nearest neighbors (O_{NN}) to the vacancies and those more distant ($O_{>NN}$) to the vacancies.

sublattices are in very good agreement with the results of earlier DFT calculations of cubic YSZ.[50,53,55]

To study the incorporation of hydrogen in the YSZ supercell the impurity was placed at various sites interstitially in the lattice. The structural optimization with the PBE functional led to 25 distinct configurations. Hydrogen was found to incorporate in two distinct manners depending on its charge state. The first type of configurations adopted for all charge states is a bond-type configuration where hydrogen forms a covalent bond OH^- with the oxygen ions [see Fig. 2(b)]. Excess protons (H^+) are exclusively stabilized in this way; that is, hydrogen defect centers in their positively charged state, H^+, can exist only in the hydroxide bond configuration. The bond length of OH^- lies typically within 0.98–0.99 Å, whereas the distance of hydrogen to the next-nearest anion has a rather wide range (from 1.70 to 2.20 Å), something that is consistent with the strong intrinsic structural disorder of the YSZ lattice. Consequently, the corresponding formation energies for these bond configurations exhibit a considerable spread of up to 1 eV. In the majority of cases encountered in the present study the amount of structural relaxation involved in the OH^- bond formation can be appreciable, especially when the oxygen ion that the hydrogen binds to is a nearest neighbor of an oxygen vacancy. In some cases the displacements of these oxygen ions can be as large as 1 Å, with a major component towards the vacant site (see Fig. 2). Such large displacements can also be considered as (at least partial) vacancy jumps induced by the impurity. As a result of these relaxations, Zr cations relatively near the oxygen vacancies are deprived of one of their anion neighbors [see circled cation in Fig. 2(b)] and become undercoordinated (sevenfold coordinated). The final defect configuration can, therefore, be viewed as a rather extended defect complex. In this respect, the cubic YSZ lattice is a far more flexible network with respect to monoclinic zirconia, in particular in its capacity to relieve the strain near the impurity by means of strong and extended lattice relaxations. In monoclinic zirconia[65] bond formation of the hydrogen with a threefold coordinated lattice oxygen leads to comparably much lower relaxations of the host lattice, which are confined to the atoms forming the bond (displacements do not exceed 0.25 Å for any ion).

Examination of 15 different bond-type configurations in various positions within the supercell showed that hydrogen binds more favorably with those oxygen ions, O_{NN}, that are nearest neighbors to the oxygen vacancies. For these configurations the accompanying lattice relaxation is also very high with these anions, O_{NN}, displacing towards the oxygen vacancy and the nearby hydrogen. In the final relaxed geometries hydrogen is bound to O_{NN} with the latter adopting a bridging-type -Zr-O_{NN}-Zr- configuration [see Fig. 2(b)]. Effectively, the anions O_{NN} in these configurations have a cation coordination of two with typical Zr-O_{NN} distances in the range of 2.10–2.30 Å. The third cation neighbor of O_{NN} [of its initial neighbor shell in the undoped fluorite lattice; designated by the dotted circle in Fig. 2(b)] is found at longer distances (typically between 2.45 to 2.85 Å), namely beyond the nearest-neighbor shell of O_{NN}. For the neutral and positively charged states of hydrogen, these configurations with the threefold coordination of the host anion O_{NN} (two Zr cations of the host plus the hydrogen) were found consistently to have among

the lowest-formation energies among all possible bond-type configurations in the YSZ lattice. Similar tendencies were also observed in the disordered transition region of $Si/SiO_2/HfO_2$ gate stacks with the proton attaching more favorably to twofold coordinated oxygen anions.[35,66]

Hydrogen in its neutral (H^0) and negative (H^-) charge states was further found to adopt additional configurations. These were interstitial configurations with hydrogen residing at high-symmetry interstitial sites of the YSZ lattice. In total, ten such configurations were determined. The first type of these sites comprise the centers of the empty cubes formed by the anion sublattice, and these are referred to as cube-centered (cc) sites in the remainder of the paper (see Fig. 2). The impurity in these cc sites has either eight or seven anion nearest neighbors, depending on the presence of anion vacancies. A second type of a stable site for both H^0 and H^- are the oxygen-vacancy sites V_O that can also be viewed as interstitial sites in the present context. These structural vacancies are part of the bulk equilibrium structure of YSZ and are not defects in the traditional sense. They compensate the charge of the substitutional yttrium and their introduction is needed to stabilize the cubic fluorite phase. The present calculations for a number of YSZ cells with different V_O configurations showed that hydrogen (H^0 and H^-) can be stabilized in almost all of these V_O sites without the need to form a short bond with a neighboring anion, since the latter remain sufficiently far away. The anion coordination for hydrogen in these sites is equal to six. For the neutral paramagnetic hydrogen, H^0, these interstitial configurations possess higher formation energies with respect to the neutral bond-type configurations by as much as 1 eV. In contrast, negatively charged hydrogen, H^- displays a clear preference for the interstitial sites with much lower formation energies (up to 2 eV) with respect to nearby negatively charged configurations of the bond type.

For the neutral state, H^0, the presence of hydrogen in these interstitial sites induces a very small interaction with the surrounding network with minimal structural relaxation: The largest ionic displacements with respect to the bulk-lattice positions do not exceed 0.15 Å. In contrast, the negatively charged H^- caused large relaxations with a tendency to maximize its distances from all its oxygen nearest neighbors and at the same time to stay close to neighboring Zr cations owing to their electrostatic attraction (either to single Zr cations or by forming bridging -Zr-H-Zr- configurations) with typical Zr-H distances in the range of 2.00–2.20 Å.

Due to the strong structural disorder of the YSZ lattice it is difficult to assess the role of yttrium ions on the energetics and local environment of hydrogen. The fact that the lower-energy bond-type hydrogen configurations were found to form near the oxygen vacancies V_O suggests that yttrium (always located at least 4 Å far away from the vacancies; see Fig. 1) does not interact with hydrogen through short-range electrostatic forces. Its influence will be through the long-range lattice relaxation that it induces due to its larger size: The nearest-neighbor Y-O distances are in the range of 2.23–2.55 Å; namely, they are considerably larger to the Zr-O distances, which are typically within 2.10–2.30 Å (the nearest-neighbor Zr-O distance in the ideal, unrelaxed fluorite cell is equal to 2.24 Å). The same can be argued for the interstitial H^0 and H^- configurations where hydrogen occupies the V_O sites. On the other hand, yttrium is closer to hydrogen when the latter occupies the cc sites in its H^0 and H^- states. Nonetheless, even in this case the nearest-neighbor shell of hydrogen comprises the ions of the oxygen sublattice [see Fig. 2(b)]. In all examined cc configurations the negatively charged H^- was always seen to approach the positively charged Zr cations since the yttrium ions carry a negative charge (yttrium substitutes the higher-valence Zr).

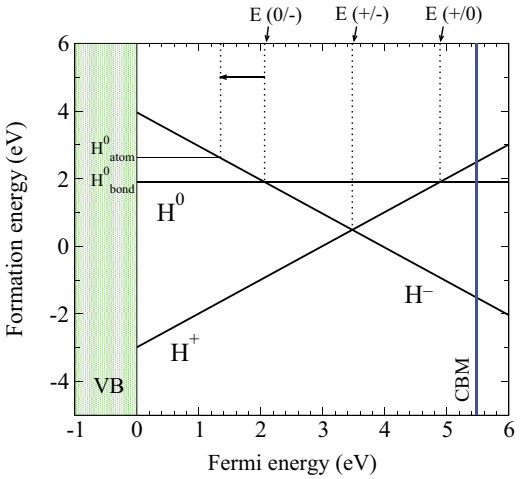

FIG. 4. (Color online) Formation energies of the neutral and charged states of hydrogen versus the Fermi-level position in the gap. The plot shows the results of the hybrid (HSE06) calculations. The thermodynamic charge-transition levels, $E(q/q')$, are denoted by the vertical lines. The reference energy for the Fermi level is set to the valence-band (VB) maximum of the bulk supercell. The thicker vertical line marks the position of the conduction-band minimum (CBM). The plot depicts the formation energies of the lowest-energy structures encountered in the YSZ cell for each H configuration and charge state.

The formation energies of the neutral and charged states of hydrogen are shown in Fig. 4 as a function of the Fermi-level position in the gap. Although the more accurate HSE06 results will be presented and discussed, the DFT-PBE results were qualitatively similar but with quantitative differences in the magnitude of the band gap and the position of the transition levels with respect to the band edges. The value of the band gap, E_{gap}, was determined to be equal to 5.47 eV from the hybrid-functional HSE06 approach for the specific YSZ cell used in the defect calculations. This value is within the range of reported experimental results[20,55] for the YSZ gap (ranging from 5.2 to 5.8 eV) and in accordance with previous *ab initio* calculations[55] with the hybrid B3LYP functional (5–5.6 eV). For the neutral case the two different types of hydrogen configurations are both indicated (two typical configurations were chosen). The plot also depicts the resulting thermodynamic charge-transition levels, $E(q/q')$, denoted by the vertical lines. These levels were obtained by considering only the lowest-energy structures for a given charge state of hydrogen, for instance the bond-type configuration for the neutral H^0 state. Similarly, the energy line for the negative state, H^-, in Fig. 4 corresponds to the lower-energy interstitial configuration of H^-, not to its higher-energy bond-type one.

It can be inferred that hydrogen is a negative-U defect where the donor level, $E(+/0)$, lies higher in energy with respect to

the acceptor level, $E(0/-)$. The obtained magnitude of $|U|$, where $|U| = |E(0/-) - E(+/0)|$, is equal to 2.83 eV.

The value of $|U|$ obtained here is slightly larger to the value of $|U|$ (2.7 eV) for hydrogen in the monoclinic phase of hafnia determined by means of DFT-GGA calculations,[67] although another DFT-GGA study[68] for the same system cites a much smaller value (1.6 eV). In Ref. 20 it was argued on the basis of their μSR data that the expected values of $|U|$ for both zirconia and hafnia should be similar to or larger than the higher value of $|U|$ reported[67] for monoclinic hafnia (2.7 eV).

The negative-U character of hydrogen and the obtained ordering of the thermodynamic transition levels suggest that the neutral state of isolated hydrogen (H^0) is never the equilibrium state at any value of the Fermi level. The transition level, $E(+/-)$, (also known as the pinning level[14]) lies deep in the band gap, at 2.0 eV with respect to the conduction-band minimum (CBM). These findings show that isolated hydrogen is an amphoteric impurity in 10.3 mol% cubic YSZ, contradicting the behavior of hydrogen in the undoped cubic zirconia lattice where a shallow-donor character was predicted.[11,12]

It is also interesting to note that the existing *ab initio* studies of isolated hydrogen in the monoclinic phase of zirconia lead to contradictory predictions concerning the behavior of hydrogen: The DFT results of Mantz and Gemmen[63] obtained at the GGA level showed that hydrogen acts exclusively as a donor, whereas the most recent hybrid-functional (HSE) calculations of Lyons *et al.*[42] predict that hydrogen is an amphoteric defect placing the H(+/−) level at almost 1 eV with respect to the CBM. The latter calculation is in agreement with the universal pinning model for hydrogen[13] whereby the transition level, $E(+/-)$, for monoclinic zirconia is also predicted to lie in the upper half of the gap, almost 1 eV below the CBM.[14] The margin of error for this result, nonetheless, must depend on the accuracy of experimental electron affinities for zirconia that were used to position the CBM with respect to the vacuum level.[14]

From the present results it can also be seen that the thermodynamic acceptor level, $E(0/-)$, is found deep in the gap, at 2.06 eV with respect to the VBM (see Fig. 4). Alternatively, even if the higher-energy interstitial configuration (H_{atom}) is taken for the neutral hydrogen state when calculating the charge transition level with the negative state, the resulting acceptor level is displaced closer to the valence band but still remains a deep level nonetheless (at 1.35 eV with respect to the VBM; see Fig. 4).

The donor level, $E(+/0)$, is also found deep inside the gap, at 0.58 eV with respect to the CBM, suggesting that the donor configuration is a deep one and not a shallow-donor type; therefore, thermal ionization is very unlikely. This finding appears to be in contradiction to earlier interpretations and analyses of the μSR data in cubic YSZ, where shallow-donor muonium states were proposed from indirect evidence with corresponding ionization energies estimated to be in the range of 10 to 30 meV.[20] In the light of the present results this issue needs to be revisited.

If one takes the distance of the thermodynamic donor level from the CBM as a measure of the donor-ionization energy then it can also be considered as the activation energy for the conversion of the paramagnetic H^0 to the diamagnetic H^+ fraction. If neutral hydrogen is instead stabilized in the higher-energy atomlike interstitial configuration, then a site change is also necessary to bring the atomlike H^0 to the donor bond-type site (see Sec. IV); this would require the crossing of an energy barrier and the migration energy for this site change needs to be determined and added to the donor-ionization energy in order to obtain the full activation energy for the conversion to the H^+ fraction.

B. Defect-induced levels in the gap

Hydrogen in the positively charged state does not introduce any defect levels in the gap since the bonding and antibonding levels of the dative OH^- bond state lie below (above) the valence (conduction) band edges, respectively, in agreement with previous calculations of H^+ in oxides.[7,10,11,13,17]

For the case of neutral paramagnetic hydrogen, H^0, defect levels appear in the gap whose position and character were found to be intimately connected with the type of site that hydrogen occupies in the YSZ lattice. These observations were mainly made by means of the much-less-elaborate DFT-PBE calculations, where the position and character of the defect levels were inspected for a large number of neutral hydrogen configurations. Nonetheless, the main trends were confirmed to hold for a few representative cases where the hybrid-functional approach was employed and the analysis that follows is only restricted to these results from the hybrid-functional calculations.

When hydrogen occupies an interstitial site, namely a cc site or the oxygen-vacancy site the induced defect levels are deep levels: The singly occupied levels of the majority spin appear consistently in the lower part of the gap, within 1 eV from the VBM (see Fig. 5).

Examination of the partial charges for individual electron bands showed that the excess electron in these levels is strongly localized on hydrogen and maintains an atomic 1s character with some 2p-type contributions on the nearest-neighbor oxygen ions (see Fig. 6). These latter contributions are consistent with the fact that the level is close to the valence band since the upper part of this band is mainly composed of oxygen 2p states. Figure 6 depicts the localized defect state for the case where hydrogen occupies a V_O site; the p-type character of the electron charge on the six oxygen nearest neighbors of hydrogen is evident.

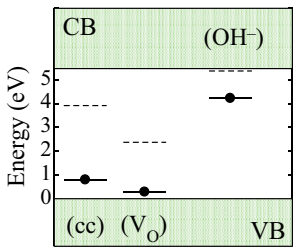

FIG. 5. (Color online) Band diagram showing the position of the occupied defect levels (majority spin; solid lines) in the gap for the different neutral hydrogen configurations: the atomlike interstitial (cc and V_O) and the bond-type (OH^-) configurations. Dashed lines denote the unoccupied levels of the minority spin. The results were obtained from the hybrid (HSE06) calculations.

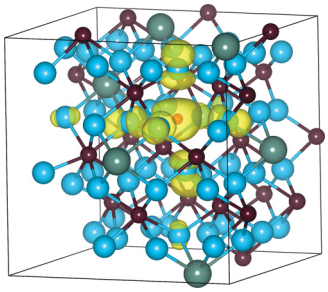

FIG. 6. (Color online) Electron-density isosurface (in yellow) for the defect state of the neutral interstitial hydrogen configuration. The plot depicts the cubic supercell and the charge isosurface for the occupied defect level in the gap. The results were obtained from the hybrid (HSE06) calculations. In the case shown here hydrogen resides in the oxygen-vacancy site. The chemical elements are represented as follows: H (small red sphere in the middle), Zr (smaller dark-gray spheres), O (larger blue spheres), Y (very large light-gray spheres). The same conventions apply for the figure that follows.

On the other hand, the defect-induced levels for the neutral bond-type configurations appear in the upper half of the gap, at about 1 eV from the conduction-band edge (see Fig. 5). No stable delocalized solution was found for these donor hydrogen configurations (whereby the excess electron would occupy the bottom of the CBM and would be delocalized in the entire supercell) using either the semilocal PBE or the hybrid HSE06 functional approach. For the specific case depicted in Fig. 5 (which shows HSE06 results) the majority-spin singly occupied defect level is at 1.2 eV with respect to the CBM. The obtained isosurface plot for this deep level showed that the unpaired electron is not centered on hydrogen (see Fig. 7). Instead it is of 4*d* character and is localized assymmetrically at neighboring Zr cations carrying also considerable weight in the interstitial space of the empty cube of the anion sublattice. Among these Zr cations, the largest electron charge is found on the undercoordinated Zr cation (sevenfold coordinated) that lost an oxygen neighbor after the introduction of the impurity [circled cation in Fig. 2(b)]. This cation is located at approximately 4 Å towards the lower-right direction with respect to the hydrogen site (see Figs. 2 and 7). Examination of the relaxed coordinates of the H^+ and H^0 bond-type configurations revealed polaronic distortions around this undercoodinated Zr cation. The excess electron polarizes the system locally by increasing the nearest-neighbor Zr-O distances (in the range 2.13–2.40 Å in the H^0 configuration) with respect to the initial positively charged H^+ configuration where these distances were in the range of 2.07–2.27 Å.

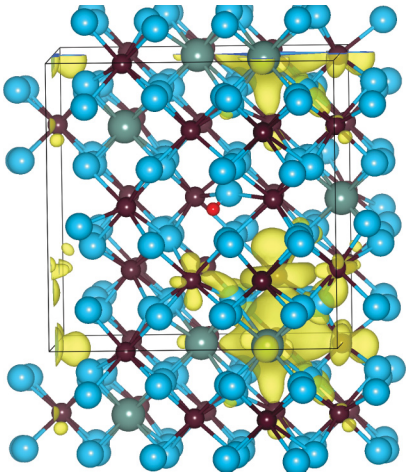

FIG. 7. (Color online) Electron-density isosurface (in yellow) for the defect state of the neutral bond-type hydrogen configuration. The plot depicts the cubic supercell and the charge isosurface for the occupied defect-induced level in the gap. The results were obtained from the hybrid (HSE06) calculations.

The present findings clearly show an intimate connection between the electron trapping near the defect in these bond-type OH^- configurations and the distinct displacements brought about by the stabilization of hydrogen in such OH^- configurations near the oxygen vacancies (see Fig. 2). Therefore, the resulting deep levels in the gap are hydrogen-induced levels but with polaronlike distortions also present (increase of the local Zr-O distances). Purely intrinsic (without hydrogen) electron trapping at different locations in the supercell caused by the structural disorder of the YSZ lattice cannot be excluded. Indeed, electron trapping was predicted for different paramagnetic centers in both intrinsic and extrinsic (Ti-doped) cubic YSZ from DFT calculations.[55] The trapped electron was observed to occur at defect complexes that consisted of specific cation (Zr^{3+} or Ti^{3+}) and oxygen-vacancy arrangements, which are clearly distinct from the hydrogen-induced complexes seen here.

The magnitudes of the thermodynamic donor level $E(+/0)$ (equal to $E_{\mathrm{CBM}} - 0.58$ eV) and acceptor level $E(0/-)$ (equal to $E_{\mathrm{VBM}} + 2.06$ eV) for hydrogen provide the thermal ionization energies for the donorlike and acceptorlike transitions, respectively,

$$H^0_{\mathrm{bond}} \rightarrow H^+_{\mathrm{bond}} + e_{\mathrm{cb}} \tag{2}$$

and

$$H^0_{\mathrm{bond}} \rightarrow H^-_{\mathrm{atom}} + h_{\mathrm{vb}} \tag{3}$$

where the different charge states of hydrogen are exclusively referred to their lower-energy configurations. e_{cb} denotes the electron excited from the donor level of H^0_{bond} to the conduction band and h_{vb} the hole created at the valence band following the transition of an electron from the valence band to the defect level of H^0_{bond}. These large values of the thermodynamic charge-transition levels suggest that conversion of the initial paramagnetic H^0 to the diamagnetic positive (H^+) and negative (H^-) hydrogen states by thermal excitation of electrons to and from the band edges is very unlikely. Equally large ($E_{\mathrm{VBM}} +$ 1.35 eV) is the magnitude of the modified acceptor level, if both H^0 and H^- are assumed to stabilize at their interstitial atomlike configurations (see Fig. 4).

The optical ionization energies for both donor and acceptor transitions will be even higher compared to the thermodynamic (also known as thermal) ionization energies. Optical ionization processes occur instantaneously (according to the Franck-Condon principle) and the obtained ionization energies are always higher owing to the neglect of the lattice relaxation: The lattice does not have the necessary time to relax and lower its energy following the electron/hole excitation.[69]

Therefore, the optical transition levels will be even deeper rather than shallower compared to the thermal, thermodynamic levels.

The conversion energies to the diamagnetic fractions (H^+ or H^-) can also be even higher: In the donor process (which should be easier given the smaller distance of the donor level from the conduction band) if neutral H^0 is initially stabilized in an interstitial atomlike configuration (H^0_{atom}) then the relevant activation energy towards H^+ should further include the migration-energy barrier for the site change to the donor bond-type (H^0_{bond}) configuration. The magnitude of these barriers are discussed in the following section.

IV. GLOBAL STABILITY AND MIGRATION PATHS OF NEUTRAL HYDROGEN

The fact that hydrogen is a negative-U defect means that its neutral state is never the thermodynamically favorable state for any value of the Fermi level in the gap. Therefore, the neutral state cannot be accessed by experimental techniques that probe thermodynamic-equilibrium conditions. Nonetheless, this does not mean that the neutral state is unstable. Indeed the present calculations and previous DFT- and Hartree-Fock-based calculations[70–74] of negative-U hydrogen in other semiconducting solids showed that neutral, paramagnetic hydrogen configurations can be well-defined local minima and therefore stable states. Experimental techniques, such as the μSR spectroscopy (with which the present study aims to provide comparisons) and optical spectroscopies can probe stable neutral H^0 states that do not normally exist at thermodynamic equilibrium but can, nonetheless, exist under conditions where thermodynamic equilibrium is not attained, namely sufficiently low temperatures and transient conditions of short lifetimes.

As discussed in the previous section, two distinct paramagnetic hydrogen configurations exist with hydrogen residing in different locations in the YSZ lattice: the deep-donor bond-type configurations that possess lower formation energies and the atomlike interstitial configurations that have higher energies but are, nonetheless, local-energy minima. NEB calculations were performed to gain an insight on the site interplay between these two different types of configurations. Specific migration pathways that connect these configurations were examined and the corresponding MEPs and classical barriers of migration were determined.

Since the positively charged state, H^+, adopts exclusively bond-type configurations it is clear that site changes of hydrogen towards this configuration will be necessary during the conversion of the paramagnetic to the (positive) diamagnetic fraction inferred from the μSR measurements.[20] The NEB calculations, therefore, can shed light on the ease of accessing these donor configurations during the conversion process by determining the activation energies for the site changes of H^0.

Two different sets of NEB calculations were performed. The first one (Sec. IV A) aimed to study locally the transition pathways and associated barriers between nearby interstitial and bond-type H^0 configurations. Although these calculations can be very informative regarding the atomic-level rearrangements involved, nonetheless, cannot describe adequately the global aspects of migration of H^0 governing long-range diffusion. For this reason, in the second set of NEB calculations (Sec. IV B) a more global picture of the migration behavior of neutral H^0 was explored. Several distinct pathways were considered that connect the various types of interstitial configurations of H^0 spanning longer distances near and further away from the oxygen vacancies.

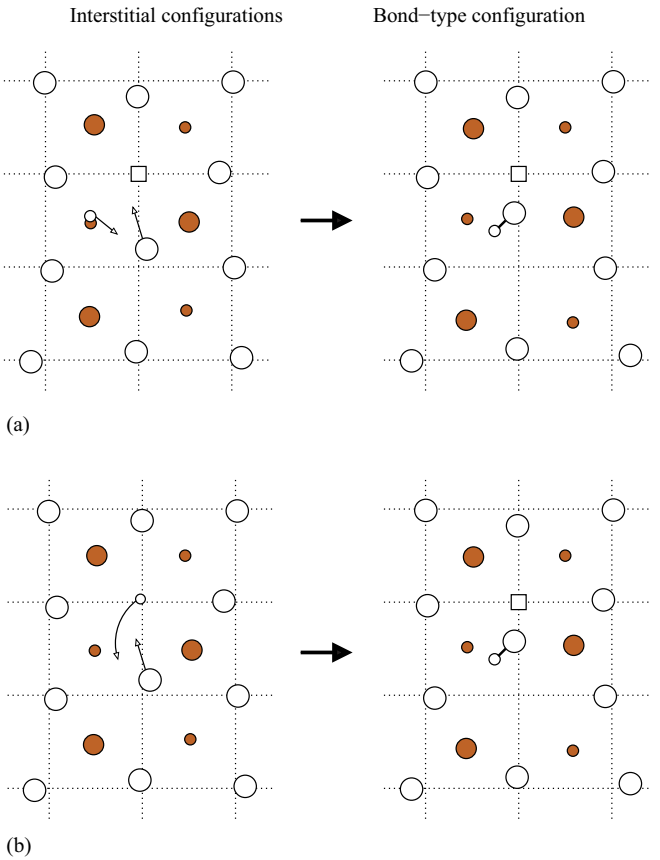

FIG. 8. (Color online) Schematics of interstitial-to-bond site changes for the neutral paramagnetic state, H^0, of hydrogen. Two representative cases are shown. (a) Hydrogen occupies initially a cc interstitial site. (b) Hydrogen occupies initially an oxygen-vacancy (V_O) interstitial site. The arrows denote the dominant atomic displacements during the site changes. Symbols as in Fig. 2.

A. Interstitial-to-bond site changes and energy barriers

The structural changes needed to transform an interstitial H^0 configuration to a nearby bond-type H^0 configuration consist of concerted (simultaneous) displacements of both the hydrogen and the anion that it eventually binds to. Two representative cases of such site changes are depicted in Fig. 8, where it can be seen that initially H^0 occupies a cc interstitial site (a) and an oxygen-vacancy site (b).

The first site change (a) depicted in Fig. 8 is the most common case encountered owing to the much larger availability of the interstitial cc sites in the YSZ lattice. Both site changes, as shown in Fig. 8, involve simultaneous displacements of both the H^0 itself and a nearby oxygen ion (depicted by the arrows).

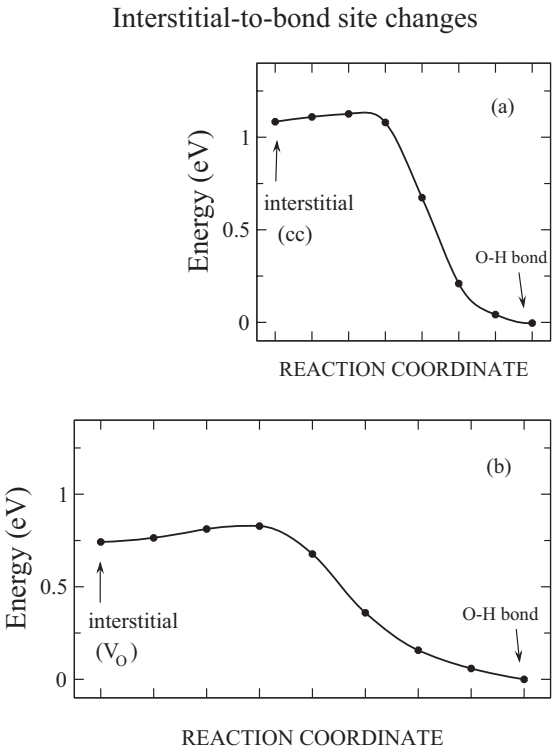

FIG. 9. Energy profiles along the MEP of the site changes of H^0 depicted in Fig. 8. The curves were obtained from numerical interpolation (Akima method) of the NEB data (circles). MEP and energies were obtained from the NEB method. The differences in the scale of the reaction coordinate reflects the fact that the hydrogen in process (b) has to displace more to complete the path (see Fig. 8).

The displacements are both short range with magnitudes in the range of 1 to 2 Å.

The migration-energy profiles along the calculated MEP for the described interstitial-to-bond site changes are shown in Fig. 9. The energy profiles for either case clearly show that hydrogen in the interstitial configurations finds itself in wide and rather flat and shallow potential wells. The energy barriers of detrapping are very small (of the order of 0.1 eV) and comparable with the calculated zero-point energy of hydrogen at the interstitial configurations (equal to 0.10 eV). Therefore, these interstitial configurations can very easily transform (even at low temperatures aided by quantum-mechanical tunneling) to the bond-type ones. It will be even easier for the much lighter muonium. The strong asymmetry in the energy profiles of Fig. 9 leads also to another aftereffect: Once hydrogen is stabilized in the donor bond site, it will be extremely difficult to migrate back to the interstitial site at least taking the same direct path. The calculated zero-point energy of hydrogen at the donor bond-type configuration is 0.31 eV and is clearly not enough to overcome the larger (in the reverse sense) barriers of the paths shown in Fig. 9. These larger barriers for hydrogen to leave its bond-site configuration reflect the fact that the bond-breaking process requires high energies. For the specific paths depicted in Fig. 8 the hop from a bond site to an interstitial site can only be achieved when hydrogen is excited to one of its higher vibrational states.

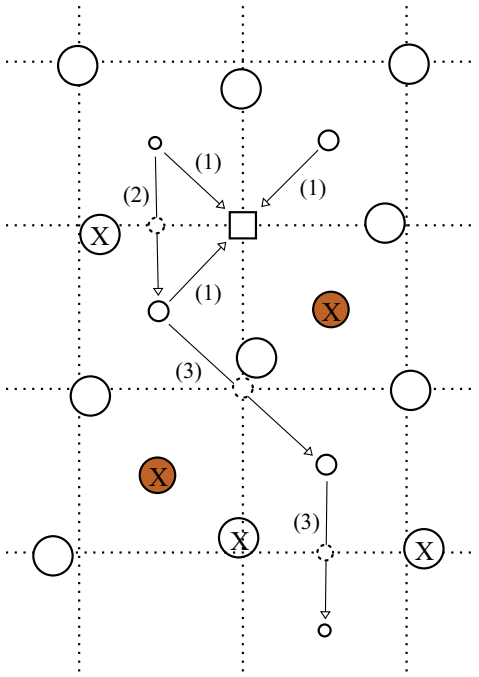

FIG. 10. (Color online) Representative migration paths (depicted by arrows) connecting the interstitial H^0 configurations. The meaning of paths denoted by (1), (2), and (3) is explained in the text. Dotted circles denote intermediate hydrogen positions midway along the paths. The circles with the X symbol denote the ions closest to H^0 midway along the paths. For purposes of clarity only two Zr ions are shown.

B. Migration paths connecting interstitial sites and energy barriers

Representative migration paths that connect interstitial H^0 configurations are schematically depicted as the arrows in Fig. 10. For these paths the resulting MEP and barriers were calculated initially by allowing full relaxation of the host lattice in response to the migrating hydrogen; corresponding results for this case are depicted by solid lines in Fig. 11. However, given the fact that hydrogen (and muonium even more) is much lighter compared to the ions of the host lattice, MEP and barriers were also determined by keeping the host lattice rigid during the hydrogen migration processes studied here. These results are depicted by the dashed lines in Fig. 11. This assumption also may describe better the actual experimental conditions attained during muonium spectroscopy; namely, the muon implantation process coupled with the small lifetime of muon (2.2 μs) may not always allow the host lattice to relax and rearrange itself into a new equilibrium configuration with the implanted species before the latter decays.

The first type of paths for the migrating hydrogen are spatially localized near the oxygen-vacancy sites. These are of the type denoted by (1) in Fig. 10 with a multiplicity of four per oxygen vacancy. In these paths hydrogen moves from its position at the cc interstitial sites to the nearest oxygen vacancy site by displacing along ⟨111⟩ directions. The energy profiles for the MEP of this type of paths are asymmetric (top panel in Fig. 11) since H^0 occupying the oxygen-vacancy sites were found to possess slightly lower

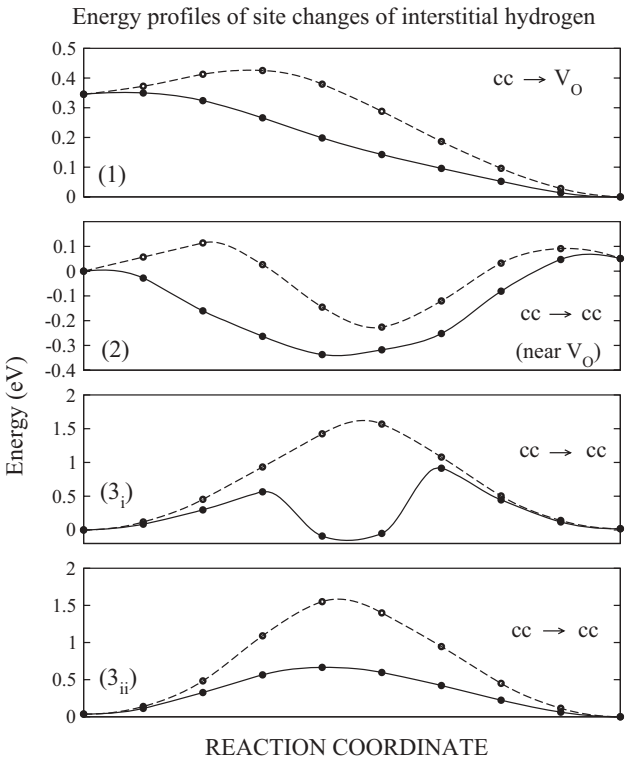

FIG. 11. Energy profiles along MEP connecting representative interstitial configurations of neutral paramagnetic hydrogen, H^0. Dashed lines denote results with H^0 migrating in a rigid host lattice. The curves were obtained from numerical interpolation (Akima method) of the NEB data (circles).

energies. The obtained barriers for hydrogen moving towards these sites (from all the neighboring cc interstitial sites) are also extremely low, indicating that these transition pathways are nearly spontaneous and can be operative even at very low temperatures (below room temperature). Therefore, H^0 can very easily migrate towards the oxygen-vacancy sites and occupy them when it initially resides in the neighboring cc interstitial sites. It is interesting also to note that these migration paths effectively connect atomlike H^0 configurations and there is no evidence from the calculated MEP that H^0 can possibly be trapped in any other type of configuration at any point along the transition pathways (see Fig. 11).

Paths of types (2) and (3) depicted in Fig. 10 connect adjacent cc interstitial H^0 configurations. The difference between paths (2) and (3) is that the former occur near an oxygen-vacancy site, whereas paths of type (3) away from it (at least beyond its nearest-neighbor neighborhood). For both of these paths hydrogen migrates along ⟨110⟩ directions and needs to pass midway between an O-O edge of the cube of the anion sublattice in order to cross over to the adjacent cube (the anions of these O-O edges are designated with the X symbol in Fig. 10). For the paths of type (2), however, in the vicinity of the oxygen vacancy V_O the crossing O-O edge simply becomes an O-V_O edge (see Fig. 10).

The NEB calculations for a number of paths of types (2) and (3) showed that these paths display two distinct behaviors in terms of the position of the transition state in their MEP: In all of the paths of type (2) and in some paths of type (3) [denoted as (3i) in Fig. 11] a potential well develops approximately midway along the path with two energy maxima in both sides of the well (see Fig. 11). The barriers for these maxima are also considerably smaller for the paths of type (2), namely those near the oxygen vacancy, whereas for the paths of type (3i) the barriers can easily be up to 1 eV (see solid-line curves in the two middle panels of Fig. 11).

It can also be seen that the minimum of the potential well in these MEP is lower than the energies of the two endpoints of the path, namely the initial and final interstitial H^0 configurations. This result shows that H^0 when migrating along these paths finds itself in lower-energy configurations that effectively act as transient trapping regions. This is not surprising since the atomlike interstitial configurations represent high-energy local minima for H^0 in YSZ and transitions among these can cause hydrogen to access lower-energy states of the configurational energy space. Inspection of these intermediate potential-well states showed that hydrogen is located very close to an anion of the crossing O-O edge (or the anion of the O-V_O edge). Upon allowing energy minimization only for these states these were always found to transform to bond-type configurations with the hydrogen bound to the nearby anion.

The remaining paths of type (3) (denoted by the subscript *ii* in the lowermost panel of Fig. 11) are characterized by a single transition state located midway along the path while the hydrogen is attempting to cross the O-O edge. The corresponding energy barriers were found to be at least 0.5 eV (the barrier for the specific path shown in Fig. 11 is equal to 0.67 eV). No precursor metastable states, therefore, occur in this case and H^0 migrates towards the interstitial site of the adjacent anion cube once it overcomes the transition-state saddle point.

The present NEB results of the migration energetics of H^0 in YSZ outline the importance of oxygen vacancies and lattice relaxation in the migration process. By decreasing the barriers of migration of interstitial H^0 they essentially make it easier for atomlike H^0 to access lower-energy intermediate states along the paths facilitating therefore site changes for hydrogen and causing the conversion to the donor bond-type paramagnetic component. The NEB results for the MEP and barriers plotted in Fig. 11 clearly show that the rigid-lattice condition has an effect on both the shape of MEP and the migration barriers: It increases the magnitude of the latter with respect to the fully relaxed results and for the paths of type (3) (away from the oxygen vacancies) does not allow the migrating H^0 to access lower-energy intermediate potential-well configurations. This shows that the local displacements of anions of the oxygen sublattice are vital to obtain such low-energy intermediate states and lower barriers: Rearrangements of the migrating hydrogen alone inside the rigid host lattice are not sufficient to provide easy (low-barrier) migration routes. The only exception was seen to occur for the transition pathways of type (2) that connect interstitial configurations in the immediate vicinity of an oxygen vacancy (see Fig. 10). For such pathways a potential well develops from the intermediate states midway along the path, similarly to the fully relaxed results (second panel in Fig. 11). It can thus be inferred that two immobile nearest-neighbor anions (the pair making up the O-O edge, denoted by X) impose severe restrictions for the migrating hydrogen to accommodate itself into low-energy geometries

midway along the path; oxygen vacancies instead can provide the necessary steric freedom for hydrogen to do so.

V. CONCLUSIONS

The present *ab initio* study with both the semilocal PBE and the hybrid HSE06 functionals shows that isolated hydrogen is an amphoteric defect in cubic 10.3 mol% YSZ with a deep transition level, $E(+/-)$, located in the upper half of the band gap. Deep thermodynamic acceptor and donor levels are predicted by the hybrid-functional approach, especially for the acceptor level, $E(0/-)$, which is found at 2.06 eV with respect to the VBM, whereas the donor level, $E(+/0)$, is at 0.58 eV from the CBM. These values suggest that thermal excitation of electrons from and to the band edges are very unlikely.

Hydrogen stabilizes in a number of different positions in the YSZ lattice with the positively charged state, H^+, forming hydroxide-bond (OH^-) configurations and the negative ion, H^-, favoring interstitial configurations maximizing its distances from the lattice oxygens. Neutral paramagnetic hydrogen is also stabilized in two distinct configurations in agreement with the existing μSR data that revealed signatures of two distinct paramagnetic muonium components.[20] The present study showed that hydrogen in its neutral state H^0 can either form bond-type configurations by binding to oxygen ions or alternatively adopt interstitial configurations of strong atomic character. The compensating oxygen vacancies were found to play an important role in the incorporation of hydrogen since they provide stable sites for hydrogen in both its negatively charged and neutral states.

Both of the distinct paramagnetic configurations of hydrogen are deep-level configurations. The position and character of the defect-induced states in the gap were seen to be intimately connected with the location where hydrogen resides in the lattice. For the atomlike interstitial configurations the excess electron is localized at the impurity site with an important degree of delocalization to the nearest-neighbor oxygen ions and with the singly occupied defect levels very close to the VBM. On the other hand, the bond-type configurations are characterized by singly occupied defect levels positioned at about 1 eV from the CBM with the excess electron asymmetrically localized at neighboring Zr cations, most notably to the undercoordinated cation that lost an oxygen neighbor following the introduction and relaxation of the impurity at the bond OH^- site. Polaronic distortions consisting of the increase of the local Zr-O distances are necessary to trap the excess electron near the Zr ion.

The present NEB results of MEP and classical barriers for migration of neutral H^0 show that thermal conversion of the atomlike interstitial H^0 to a lower-energy nearby bond-type H^0 configuration is very likely with very low energy barriers. Nonetheless, this is true only if the local environment near the migrating H^0 (in particular the anion that H^0 binds to) has the necessary time to rearrange itself.

A more global picture of the long-range migration behavior of H^0 was also explored by considering alternative longer-range migration routes connecting directly atomlike H^0 from adjacent interstitial sites. Due to the intrinsic structural disorder of the YSZ lattice the activation energies of migration displayed a strong dependence on the local topology with major influences from oxygen vacancies and lattice relaxation. More specifically for migration paths beyond the nearest-neighbor shell of the vacancies, the obtained migration barriers were in the range of 0.5 to 1.5 eV, while for paths in the immediate vicinity of vacancies the corresponding barriers were much smaller. Oxygen vacancies and lattice relaxation were also found to play an important role in the interconversion between the two distinct paramagnetic configurations of hydrogen by favoring trapping of hydrogen to intermediate lower-energy potential-well states that can subsequently convert to the bond-type donor configurations of H^0.

ACKNOWLEDGMENTS

This work was supported by the program COMPETE: FCOMP-01-0124-FEDER-010450 and by the Portuguese Fundação para a Ciência e a Tecnologia (FCT) under the Ciência 2007 and PTDC/FIS/102722/2008 programs. The computer resources of the Department of Physics of the University of Coimbra were used, including the Milipeia cluster at the Laboratory for Advanced Computing. The author thanks Rui Vilão, Stephen Cox, João Gil, Alois Weidinger, and Fernando Nogueira and the Condensed Matter Physics group for fruitful discussions. CEMDRX is supported by FCT under COMPETE: PEst-/FIS/UI0036/2011 Strategic Project.

[1] D. M. Fleetwood, Microelectron. Reliab. **42**, 523 (2002).
[2] D. K. Schroder and J. A. Babcock, J. Appl. Phys. **94**, 1 (2003).
[3] M. Houssa, G. Pourtois, M. M. Heyns, and A. Stesmans, J. Phys.: Condens. Matter **17**, S2075 (2005).
[4] S. T. Pantelides, L. Tsetseris, S. N. Rashkeev, X. J. Zhou, D. M. Fleetwood, and R. D. Schrimpf, Microelectron. Reliab. **47**, 903 (2007).
[5] P. Hohenberg and W. Kohn, Phys. Rev. **136**, B864 (1964); W. Kohn and L. J. Sham, *ibid.* **140**, A1133 (1965).
[6] S. B. Zhang and D. J. Chadi, Phys. Rev. B **41**, 3882 (1990).
[7] A. Yokozawa and Y. Miyamoto, Phys. Rev. B **55**, 13783 (1997).
[8] P. E. Blöchl, Phys. Rev. B **62**, 6158 (2000).
[9] C. G. Van de Walle, Phys. Rev. Lett. **85**, 1012 (2000).
[10] Ç. Kiliç and A. Zunger, Appl. Phys. Lett. **81**, 73 (2002).
[11] P. W. Peacock and J. Robertson, Appl. Phys. Lett. **83**, 2025 (2003).
[12] J. Robertson and P. W. Peacock, Thin Solid Films **445**, 155 (2003).
[13] C. G. Van de Walle and J. Neugebauer, Nature (London) **423**, 626 (2003).
[14] C. G. Van de Walle, Physica B **376**, 1 (2006); **377**, 1 (2006).
[15] A. Zanotti and C. G. Van de Walle, Nat. Mater. **6**, 44 (2007).
[16] A. K. Singh, A. Janotti, M. Scheffler, and C. G. Van de Walle, Phys. Rev. Lett. **101**, 055502 (2008).
[17] K. Xiong, J. Robertson, and S. J. Clark, J. Appl. Phys. **102**, 083710 (2007).

[18]G. Chiodelli, F. Maglia, U. Anselmi-Tamburini, and Z. A. Munir, Solid State Ionics **180**, 297 (2009).
[19]J. S. Park, Y. B. Kim, J. H. Shim, S. Kang, T. M. Gür, and F. B. Prinz, Chem. Mater. **22**, 5366 (2010).
[20]S. F. J. Cox, J. L. Gavartin, J. S. Lord, S. P. Cottrell, J. M. Gil, H. V. Alberto, J. Piroto Duarte, R. C. Vilão, N. Ayres de Campos, D. J. Keeble, E. A. Davis, M. Charlton, and D. P. van der Werf, J. Phys.: Condens. Matter **18**, 1079 (2006).
[21]J. M. Gil, H. V. Alberto, R. C. Vilão, J. P. Duarte, P. J. Mendes, L. P. Ferreira, N. Ayres de Campos, A. Weidinger, J. Krauser, Ch. Niedermayer, and S. F. J. Cox, Phys. Rev. Lett. **83**, 5294 (1999).
[22]S. F. J. Cox, E. A. Davis, S. P. Cottrell, P. J. C. King, J. S. Lord, J. M. Gil, H. V. Alberto, R. C. Vilão, J. PirotoDuarte, N. Ayres de Campos, A. Weidinger, R. L. Lichti, and S. J. C. Irvine, Phys. Rev. Lett. **86**, 2601 (2001).
[23]R. C. Vilão, J. M. Gil, A. Weidinger, H. V. Alberto, J. Piroto Duarte, N. Ayres de Campos, R. L. Lichti, K. H. Chow, S. P. Cottrell, and S. F. J. Cox, Phys. Rev. B **77**, 235212 (2008).
[24]S. F. J. Cox, Rep. Prog. Phys. **72**, 116501 (2009).
[25]R. C. Vilão, A. G. Marinopoulos, R. B. L. Vieira, A. Weidinger, H. V. Alberto, J. P. Duarte, J. M. Gil, J. S. Lord, and S. F. J. Cox, Phys. Rev. B **84**, 045201 (2011).
[26]E. L. Silva, A. G. Marinopoulos, R. C. Vilão, R. B. L. Vieira, H. V. Alberto, J. Piroto Duarte, and J. M. Gil, Phys. Rev. B **85**, 165211 (2012).
[27]J. P. Perdew, K. Burke, and M. Ernzerhof, Phys. Rev. Lett. **77**, 3865 (1996).
[28]J. Heyd and G. E. Scuseria, J. Chem. Phys. **121**, 1187 (2004).
[29]J. Paier, M. Marsman, K. Hummer, G. Kresse, I. C. Gerber, and J. G. Angyan, J. Chem. Phys. **124**, 154709 (2006); **125**, 249901 (2006).
[30]M. Marsman, J. Paier, A. Stroppa, and G. Kresse, J. Phys.: Condens. Matter **20**, 064201 (2008).
[31]J. P. Perdew and A. Zunger, Phys. Rev. B **23**, 5048 (1981).
[32]E. R. Batista, J. Heyd, R. G. Hennig, B. P. Uberuaga, R. L. Martin, G. E. Scuseria, C. J. Umrigar, and J. W. Wilkins, Phys. Rev. B **74**, 121102 (2006).
[33]F. Oba, A. Togo, I. Tanaka, J. Paier, and G. Kresse, Phys. Rev. B **77**, 245202 (2008).
[34]E. Finazzi, C. Di Valentin, G. Pacchioni, and A. Selloni, J. Chem. Phys. **129**, 154113 (2008).
[35]P. Broqvist, A. Alkauskas, J. Godet, and A. Pasquarello, J. Appl. Phys. **105**, 061603 (2009).
[36]J. B. Varley, A. Janotti, A. K. Singh, and C. G. Van de Walle, Phys. Rev. B **79**, 245206 (2009).
[37]P. Agoston, K. Albe, R. M. Nieminen, and M. J. Puska, Phys. Rev. Lett. **103**, 245501 (2009).
[38]A. Carvalho, A. Alkauskas, A. Pasquarello, A. K. Tagantsev, and N. Setter, Phys. Rev. B **80**, 195205 (2009).
[39]P. Broqvist, A. Alkauskas, and A. Pasquarello, Phys. Status Solidi A **207**, 270 (2010).
[40]A. Janotti, J. B. Varley, P. Rinke, N. Umezawa, G. Kresse, and C. G. Van de Walle, Phys. Rev. B **81**, 085212 (2010).
[41]J. B. Varley, H. Peelaers, A. Janotti, and C. G. Van de Walle, J. Phys.: Condens. Matter **23**, 334212 (2011).
[42]J. L. Lyons, A. Janotti, and C. G. Van de Walle, Microelectron. Eng. **88**, 1452 (2011).
[43]H. Jónsson, G. Mills, and K. W. Jacobsen, in *Classical and Quantum Dynamics in Condensed Phase Simulations*, edited by B. J. Berne, G. Ciccotti, and D. F. Coker (World Scientific, Singapore, 1998), p. 385.
[44]P. E. Blöchl, Phys. Rev. B **50**, 17953 (1994).
[45]G. Kresse and D. Joubert, Phys. Rev. B **59**, 1758 (1999).
[46]G. Kresse and J. Hafner, Phys. Rev. B **47**, 558 (1993).
[47]G. Kresse and J. Hafner, Phys. Rev. B **49**, 14251 (1994).
[48]G. Kresse and J. Furthmüller, Phys. Rev. B **54**, 11169 (1996).
[49]H. Monkhorst and J. Pack, Phys. Rev. B **13**, 5188 (1976).
[50]G. Stapper, M. Bernasconi, N. Nicoloso, and M. Parrinello, Phys. Rev. B **59**, 797 (1999).
[51]C. Pascual and P. Duran, J. Am. Ceram. Soc. **66**, 23 (1982).
[52]A. Bogicevic, C. Wolverton, G. M. Crosbie, and E. B. Stechel, Phys. Rev. B **64**, 014106 (2001).
[53]S. Ostanin, A. J. Craven, D. W. McComb, D. Vlachos, A. Alavi, A. T. Paxton, and M. W. Finnis, Phys. Rev. B **65**, 224109 (2002).
[54]R. Pornprasertsuk, P. Ramanarayanan, C. B. Musgrave, and F. B. Prinz, J. Appl. Phys. **98**, 103513 (2005).
[55]F. Pietrucci, M. Bernasconi, C. Di Valentin, F. Mauri, and C. J. Pickard, Phys. Rev. B **73**, 134112 (2006).
[56]F. Pietrucci, M. Bernasconi, A. Laio, and M. Parrinello, Phys. Rev. B **78**, 094301 (2008).
[57]C. R. A. Catlow, A. V. Chadwick, G. N. Greaves, and L. M. Moroney, J. Am. Ceram. Soc. **69**, 272 (1986).
[58]B. W. Veal, A. G. McKale, A. P. Paulikas, S. J. Rothman, and L. J. Nowicki, Physica B + C **150**, 234 (1988).
[59]P. Li, I. Wei Chen, and J. E. Penner-Hahn, Phys. Rev. B **48**, 10074 (1993); J. Am. Ceram. Soc. **77**, 118 (1994).
[60]K. Kawata, H. Maekawa, T. Nemoto, and T. Yamamura, Solid State Ionics **177**, 1687 (2006).
[61]G. Makov and M. C. Payne, Phys. Rev. B **51**, 4014 (1995).
[62]A. L. Shluger, A. S. Foster, J. L. Gavartin, and P. V. Sushko, in *Nano and Giga Challenges in Microelectronics*, edited by J. Greer, A. Korkin, and J. Labanowski (Elsevier Science, Amsterdam, 2003), p. 151.
[63]Y. A. Mantz and R. S. Gemmen, J. Phys. Chem. C **114**, 8014 (2010).
[64]S. Fabris, A. T. Paxton, and M. W. Finnis, Acta Materialia **50**, 5171 (2002).
[65]A. G. Marinopoulos (unpublished).
[66]J. Godet, P. Broqvist, and A. Pasquarello, Appl. Phys. Lett. **91**, 262901 (2007).
[67]J. L. Gavartin, A. L. Shluger, A. S. Foster, and G. I. Bersuker, J. Appl. Phys. **97**, 053704 (2005).
[68]J. Kang, E. C. Lee, K. J. Chang, and Y. G. Jin, Appl. Phys. Lett. **84**, 3894 (2004).
[69]C. G. Van de Walle and J. Neugebauer, J. Appl. Phys. **95**, 3851 (2004).
[70]C. G. Van de Walle, Phys. Rev. Lett. **64**, 669 (1990).
[71]R. H. Luchsinger, Y. Zhou, and P. F. Meier, Phys. Rev. B **55**, 6927 (1997).
[72]A. R. Porter, M. D. Towler, and R. J. Needs, Phys. Rev. B **60**, 13534 (1999).
[73]J. P. Goss, J. Phys.: Condens. Matter **15**, R551 (2003).
[74]C. G. Van de Walle and J. Neugebauer, Annu. Rev. Mater. Res. **36**, 179 (2006).